Inorg. Chem. **2004**, *43*, 1273–1286

Structure, Energetics, and Bonding of First Row Transition Metal Pentazolato Complexes: A DFT Study

Athanassios C. Tsipis* and Aikaterini Th. Chaviara

Department of General and Inorganic Chemistry, Faculty of Chemistry, Aristotle University of Thessaloniki, 541 24 Thessaloniki, Greece

Received September 22, 2003

Quantum chemical calculations with gradient-corrected (B3LYP) density functional theory for the mono- and bispentazolato complexes of the first row transition metals (V, Cr, Mn, Fe, Co, and Ni), the all-nitrogen counterparts of metallocenes, were performed, and their stability was investigated. All possible bonding modes (e.g. η^1, η^2, η^3, and η^5) of the pentazolato ligand to the transition metals have been examined. The transition metal pentazolato complexes are predicted to be strongly bound molecules. The computed total bond dissociation enthalpies that yield free transition metal atoms in their ground states and the free pentazolato ligands were found in the range of 122.0–201.9 (3.7–102.3) kcal mol^{-1} for the bispentazolato (monopentazolato) complexes, while those yielding M^{2+} and anionic pentazolato ligands were found in the range of 473.2–516.7 (273.6–353.5) kcal mol^{-1}. The electronic ground states of azametallocenes along with their spectroscopic properties (IR, NMR, and UV–vis) obtained in a consistent manner across the first transition metal series provide means for discussion of their electronic and bonding properties, the identification of the respective azametallocenes, and future laboratory studies. Finally, exploring synthetic routes to azametallocenes it was found that a [2 + 3] cycloaddition of dinitrogen to a coordinated azide ligand with nickel(II) does not seem to provide a promising synthetic route for transition metal pentazolato complexes while the oxidative addition of phenylpentazole and fluoropentazole to Ni(0) bisphosphane complexes merits attention for the experimentalists.

Introduction

Very recently experimental evidence[1] revealed that the long-sought aromatic *cyclo*-N_5 anion, the all-nitrogen counterpart of the cyclopentadienide (Cp) anion, is no longer hypothetical, for it can be generated by the electrospray ionization method inside a mass spectrometer. This work opened up the possibility of studying the properties—and perhaps even the chemistry—of the pentazolato anion in the gas phase and comparing the results directly with calculations. Because the *cyclo*-N_5 anion is aromatic and isoelectronic with the Cp ligand, its coordination to transition metal atoms or ions would be expected to open an entirely new realm, the inorganic nitrogen analogues of metallocenes. Pentazole N_5H,[2] its anion N_5^-, and several Li^+ salts[3] of N_5^- and tetrazolylpentazoles[4] were the subject of various theoretical studies. Although metallocene-like structures have previously been proposed,[5] only very recently the structure, energetic properties, and bonding properties of the iron bispentazole, Fe(η^5-N_5)$_2$, complex were exhaustively investigated by Frenking's group,[6] and the complex which has D_{5d} symmetry was predicted to be a strongly bonded molecule. Frenking's group extended the investigations to the group-15 analogues [Fe(η^5-E_5)$_2$], [FeCp(η^5-E_5)], and [Ti-

* Author to whom correspondence should be addressed. E-mail: tsipis@chem.auth.gr.

(1) (a) Vij, A.; Pavlovich, J. G.; Wilson, W. W.; Vij, V.; Christe, K. O. *Angew. Chem., Int. Ed.* **2002**, *41*, 3051. (b) Östmark, H.; Wallin, S.; Brinck, T.; Carlqvist, P.; Claridge, R.; Hedlund, E.; Yudina, L. *Chem. Phys. Lett.* **2003**, *379*, 539−546.

(2) (a) Nguyen, M. T.; Ha, T.-K. *Chem. Phys. Lett.* **2001**, *335*, 311−320. (b) Wang, X.; Hu, H.-R.; Tian, A.; Wong, N. B.; Chien, S.-H.; Li, W.-K. *Chem. Phys. Lett.* **2000**, *329*, 483−489. (c) Cheng, C. *Int. J. Quantum Chem.* **2000**, *80*, 27−37. (d) Perrera, S.; Bartlett, R. J. *Chem. Phys. Lett.* **1999**, *314*, 381−387. (e) Janoschek, R. *Angew. Chem., Int. Ed. Engl.* **1993**, *32*, 230−232. (f) Ferris, K. F.; Bartlett, R. J. *J. Am. Chem. Soc.* **1992**, *114*, 8302−8303.

(3) (a) Nguyen, M. T. *Coord. Chem. Rev.* **2003**, *244*, 93−113. (b) Glukhovtsev, M. N.; Schleyer, P. v. R.; Maerker, C. *J. Phys. Chem.* **1993**, *97*, 8300−8306.

(4) Hammerl, A.; Klapotke, T. M. *Inorg. Chem.* **2002**, *41*, 906−912.

(5) (a) Nguyen, M. T.; Sana, M.; Leroy, G.; Elguero, J. *Can. J. Chem.* **1983**, *61*, 1435. (b) Nguyen, M. T.; McGinn, A. F.; Hegarty, A. F.; Elguero, J. *Polyhedron* **1985**, *4*, 1721. (c) Bartlett, R. J. *Chem. Ind. (London)* **2000**, 140.

(6) Lein, M.; Frunzke, J.; Timonshkin, A.; Frenking, G. *Chem. Eur. J.* **2001**, *7*, 4155−4163.

10.1021/ic035112g CCC: $27.50
Published on Web 01/21/2004

(η^5-E_5)$_2$] (E = P, As, Sb, Bi).[7−10] It was predicted that all π-heterocyclic complexes are stable compounds, while the metal−ligand bonding, analyzed with an energy decomposition method, was shown to come from 53−58% electrostatic attraction and 42−47% from covalent interactions. The analysis of the bonding situation and electronic structure in a series of phosphaferrocenes and azaferrocenes, using the electron localization function (ELF) methodology, revealed the importance of the heteroatom lone pair.[11] Moreover, the results of theoretical calculations on pentazole anion and various metal cation (Na^+, K^+, Mg^{2+}, Ca^{2+}, and Zn^{2+}) pentazole anion complexes[12] as well as on the Al_2N_4 and AlN_n (n = 4 to 7) precursors of high energy density materials (HEDM) have also been reported very recently.[13] In searching for stabilization of the pentazolato ligand we report herein DFT results for its interaction with first row transition metals (V, Cr, Mn, Fe, Co, and Ni). In this context, we addressed the question concerning the molecular and electronic structures, stabilities, bonding features, and spectroscopic properties of the first row transition metal azametallocenes and compared them with the corresponding properties of the respective predecessor metallocenes.

Theoretical Methods

In view of the good performance of density functional theory (DFT) for metallocenes[14] and organometallic compounds in general,[15] we were instigated to perform DFT/B3LYP calculations on all of the azametallocenes using the GAUSSIAN 98 program suite.[16] The geometries of the ligands and complexes were fully optimized at the Becke's 3-parameter hybrid functional combined with the Lee−Yang−Parr correlation functional abbreviated as the B3LYP level of density functional theory,[17,18] using the 6-31G(d,p) basis set. In all computations no constraints were imposed on the geometry. Full geometry optimization was performed for each structure using Schlegel's analytical gradient method,[19] and the attainment of the energy minimum was verified by calculating the vibrational frequencies that result in absence of imaginary eigenvalues. All the stationary points have been identified for minimum (number of imaginary frequencies NIMAG = 0) or transition states (NIMAG = 1). The vibrational modes and the corresponding frequencies are based on a harmonic force field. This was achieved with the SCF convergence on the density matrix of at least 10^{-9} and the rms force less than 10^{-4} au. All bond lengths and bond angles were optimized to better than 0.001 Å and 0.1°, respectively. The computed electronic energies were corrected to constant pressure and 298 K, for zero point energy (ZPE) differences and for the contributions of the translational, rotational, and vibrational partition functions. The natural bond orbital (NBO) population analysis was performed using Weinhold's methodology.[20] Magnetic shielding tensors have been computed with the GIAO (gauge-including atomic orbitals) DFT method[21] as implemented in the GAUSSIAN98 series of programs[16] employing the B3LYP level of theory. Time-dependent density functional theory (TD-DFT)[22] calculations were performed on the equilibrium ground state geometries employing the same density functionals and basis sets used in geometry optimization. The Davidson algorithm was used, in which the error tolerance in the square of the excitation energies and trial-vector orthonormality criterion were set to 10^{-8} and 10^{-10}, respectively. The success of TD-DFT method in calculating excitation energies of transition metal complexes has been demonstrated in several recent studies.[23]

Results and Discussion

Equilibrium Geometries of the Bispentazolato Complexes. Selected geometric parameters for the first row transition metal bispentazolato complexes computed at the B3LYP/6-31G(d,p) level of theory are shown in Figure 1.

The calculations predict that the bispentazolato complexes of V^{2+}, Cr^{2+}, Fe^{2+}, and Co^{2+} adopt an equilibrium geometry involving the η^5-bonding mode of the pentazolato ligands with the eclipsed (D_{5h}) conformation for V(η^5-N_5)$_2$, **3**, and the staggered (D_{5d}) one for Cr(η^5-N_5)$_2$, **4**, Fe(η^5-N_5)$_2$, **6**, and Co(η^5-N_5)$_2$, **7**. The staggered conformation of V(η^5-N_5)$_2$ and the eclipsed conformations of Fe(η^5-N_5)$_2$ and Co(η^5-N_5)$_2$ correspond to transition states (NIMAG = 1) with almost the same energy (energy barrier < 0.40 kcal mol^{-1}); thereby there is free rotation of the pentazolato ligands about the C_5 symmetry axis. It should be noted that the equilibrium structure of Fe(η^5-N_5)$_2$ resembles that computed at the same

(7) Frunzke, J.; Lein, M.; Frenking, G. *Organometallics* **2002**, *21*, 3351−3359.
(8) Lein, M.; Frunzke, J.; Frenking, G. *Inorg. Chem.* **2003**, *42*, 2504−2511.
(9) Lein, M.; Frunzke, J.; Frenking, G. *Angew. Chem., Int. Ed.* **2003**, *42*, 1303−1306.
(10) Frenking, G.; Wichmann, K.; Fröhlich, N.; Loschen, C.; Lein, M.; Frunzke, J.; Rayón, V. M. *Coord. Chem. Rev.* **2003**, *238*−*239*, 55−82.
(11) Frison, G.; Mathey, F.; Sevin, A. *J. Phys. Chem. A* **2002**, *106*, 5653−5659.
(12) Burke, L. A.; Butler, R. N.; Stephens, J. C. *J. Chem. Soc., Perkin Trans.* **2001**, *2*, 1679−1684.
(13) Lee, E. P. F.; Dyke, J. M.; Claridge, R. P. *J. Phys. Chem. A* **2002**, *106*, 8680−8695.
(14) Xu, Z.-F.; Xie, Y.; Feng, W.-L.; Schaefer, H. F., III. *J. Phys. Chem. A* **2003**, *107*, 2716−2729.
(15) Ziegler, T. *Can. J. Chem.* **1995**, *73*, 743.
(16) Frisch, M. J.; Trucks, G. W.; Schlegel, H. B.; Scusseria, G. E.; Robb, M. A.; Cheeseman, J. R.; Zakrzewski, V. G.; Montgomery, J. A.; Stratmann, R. E.; Burant, J. C.; Dapprich, S.; Millan, J. M.; Daniels, A. D.; Kudin, K. N.; Strain, M. C.; Farkas, O.; Tomasi, J.; Barone, V.; Cossi, M.; Cammi, R.; Mennucci, B.; Pomelli, C.; Adamo, C.; Clifford, S.; Orchterski, J.; Petersson, G. A.; Ayala, P. Y.; Cui, Q.; Morokuma, K.; Malick, D. K.; Rabuck, A. D.; Raghavachari, K.; Foresman, J. B.; Cioslowski, J.; Ortiz, J. V.; Stefanov, B. B.; Liu, G.; Liashenko, A.; Piskorz, P.; Komaroni, I.; Gomperts, R.; Martin, R. L.; Fox, D. J.; Keith, T.; Al-Laham, M. A.; Peng, C. Y.; Nanayakkara, A.; Gonzalez, C.; Challacombe, M.; Gill, P. M.; Johnson, P.; Chen, W.; Wong, M. W.; Andres, J. L.; Head-Gordon, M.; Replogle, E. S.; Pople, J. A. *Gaussian 98*, revision A.7; Gaussian Inc.: Pittsburgh, PA, 1998.
(17) Lee, C.; Yang, W.; Parr, R. G. *Phys. Rev. B* **1988**, *37*, 785−789.
(18) Becke, A. D. *J. Chem. Phys.* **1993**, *98*, 5648−5652.
(19) Schlegel, H. B. *J. Comput. Chem.* **1982**, *3*, 214.
(20) (a) Reed, A. E.; Curtiss, L. A.; Weinhold, F. *Chem. Rev.* **1988**, *88*, 899−926. (b) Weinhold, F. In *The Encyclopedia of Computational Chemistry*; Schleyer, P.v. R., Ed.; John Wiley & Sons: Chichester, 1998; pp 1792−1811.
(21) (a) Ditchfield, R. *Mol. Phys.* **1974**, *27*, 789. (b) Gauss, J. *J. Chem. Phys.* **1993**, *99*, 3629.
(22) (a) van Gisbergen, S. J. A.; Kootstra, F.; Schipper, P. R. T.; Gritsenko, O. V.; Snijders, J. G.; Baerends, E. J. *Phys. Rev. A* **1998**, *57*, 1556. (b) Jamorski, C.; Casida, M. E.; Salahud, D. R. *J. Chem. Phys.* **1996**, *104*, 5134. (c) Bauernschmitt, R.; Ahlrichs, R. *Chem. Phys. Lett.* **1996**, *256*, 454.
(23) (a) van Gisbergen, S. J. A.; Groeneveld, J. A.; Rosa, A.; Snijders, J. G.; Baerends, E. J. *J. Phys. Chem. A* **1999**, *103*, 6835. (b) Rosa, A.; Baerends, E. J.; van Gisbergen, S. J. A.; van Lenthe, E.; Groeneveld, J. A.; Snijders, J. G. *J. Am. Chem. Soc.* **1999**, *121*, 10356. (c) Boulet, P.; Chermette, H.; Daul, C.; Gilardoni, F.; Rogemond, F.; Weber, J.; Zuber, G. *J. Phys. Chem. A* **2001**, *105*, 885.

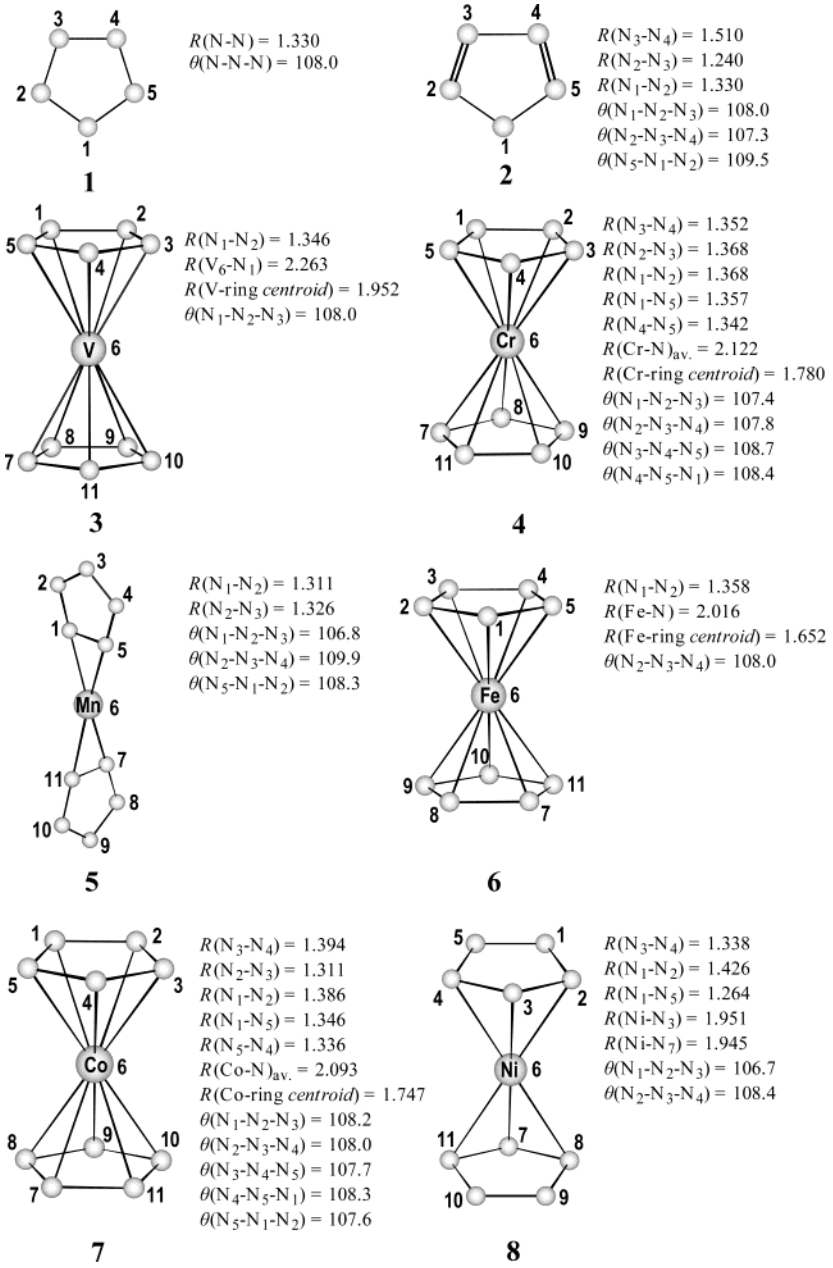

Figure 1. Equilibrium geometries of the first row transition metal bispentazolato complexes computed at the B3LYP/6-31G(d,p) level.

level of theory, using ECPs for Fe and the 6-31G(d,p) basis set for C and N atoms.[6] The computed distances between the transition metal center and the centroid of the aromatic pentazolato ring were found to be 1.953, 1.780, 1.650, and 1.747 Å for **3**, **4**, **6**, and **7**, respectively. Interestingly, the corresponding experimental values for the VCp_2, $CrCp_2$, $FeCp_2$, and $CoCp_2$ metallocenes, being 1.928(6),[24] 1.798(4),[25] 1.660,[26] and 1.739(2)[27] Å, respectively illustrate the similar bonding properties of the two ligands and predict comparable stability of their complexes. It is worth noting that the M−Cp distances for the eclipsed conformations (D_{5h}) of VCp_2, $CrCp_2$, $FeCp_2$, and $CoCp_2$ metallocenes computed at the B3LYP/DZP level of theory are 1.965, 1.896, 1.681, and 1.774 Å, respectively.

Obviously, the two pentazolato rings are closer to the Fe^{2+} ion and are perfectly parallel in $V(\eta^5\text{-}N_5)_2$ and $Fe(\eta^5\text{-}N_5)_2$, but slightly tilted in $Cr(\eta^5\text{-}N_5)_2$ and $Co(\eta^5\text{-}N_5)_2$. In contrast to manganocene $MnCp_2$, and nickelocene $NiCp_2$, which have two very low-lying conformations, the eclipsed (D_{5h}) and staggered (D_{5d}) ones, the bispentazolato complex of Mn^{2+} adopts the η^2-bonding mode of the pentazolato ligands with a tetrahedral stereochemistry (D_{2d}), while that of Ni^{2+} adopts an allyl-type η^3-bonding mode with a staggered conformation. Noteworthy is the nonplanarity of the pentazole ring in azanickelocene, which is folded along N2···N4 (N3−N4−N2−N1 flap angle of −169.8°). All attempts to

(24) (a) Haaland, A.; Lusztyk, J.; Novak, D. P. *J. Chem. Soc., Chem. Commun.* **1974**, 54. (b) Gard, E.; Haaland, A.; Novak, D. P.; Seip, R. *J. Organomet. Chem.* **1975**, *88*, 181.
(25) Almenningen, A.; Gard, E.; Haaland, A. *J. Organomet. Chem.* **1976**, *107*, 273.
(26) (a) Haaland, A.; Nilsson, J. E. *Acta Chem. Scand.* **1968**, *22*, 2653. (b) Haaland, A. *Top. Curr. Chem.* **1975**, *53*, 1. (c) Haaland, A. *Inorg. Nucl. Chem. Lett.* **1979**, *15*, 267.
(27) Hedberg, A. K.; Hedberg, L.; Hedberg, K. *J. Chem. Phys.* **1975**, *63*, 1262.

Table 1. Bond Dissociation Enthalpies ΔH_1, ΔH_2, and ΔH_3 (in kcal mol^{-1}) of the First Row Transition Metal Bispentazolato Complexes Computed at the B3LYP/6-31G(d,p) Level

	state	ΔH_1	ΔH_2	ΔH_3[a]
3	$^4A_1'$	201.9	516.7	177.2 (163.2)[b]
4	$^3A_{1g}$	162.0	511.1	182.0 (157.9)
5	^6A	188.6	511.7	(185.6)
6	$^1A_{1g}$	129.1	473.2	199.6 (195.1)
7	$^2A_{1g}$	129.7	491.8	(174.1)
8	^1A_g	122.0	511.5	175.1[c] (163.0)

[a] $\Delta H_3 = E[M(N_5)_2] - [E([MN_5]^+) + E(N_5^-)]$. [b] Figures in parentheses are the values for the dissociation to the $[M(\eta^2\text{-}N_5)]^+$ species. [c] This value is for the dissociation to the $[Ni(\eta^1\text{-}N_5)]^+$ species.

locate on the PES of $Mn(N_5)_2$ and $Ni(N_5)_2$ systems local minima corresponding to η^5-bonded eclipsed (D_{5h}) or staggered (D_{5d}) conformations were unsuccessful, since even starting the optimization with these geometries always they converged to structures **5** and **8**, respectively.

Stability of the Bispentazolato Complexes. All $M(N_5)_2$ azametallocenes are predicted to be bound with respect to their homolytic or heterolytic dissociation to M or M^{2+} and $N_5^\bullet$ or N_5^- in their ground states. The dissociation enthalpies for (i) the homolytic dissociation $M(N_5)_2 \rightarrow M + 2N_5^\bullet$, ΔH_1, (ii) the heterolytic dissociation $M(N_5)_2 \rightarrow M^{2+} + 2N_5^-$, ΔH_2, and (iii) the dissociation $M(N_5)_2 \rightarrow [M(N_5)]^+ + N_5^-$, ΔH_3, are collected in Table 1.

It can be seen that the $M(N_5)_2$ complexes have relatively high metal−ligand bond energies, which might be sufficiently large to allow stabilization of the pentazole molecule. Notice that the dissociation energies of the cationic metallocenes Cp_2M^+ (M = V, Cr, Mn, Fe, Co, Ni) to CpM^+ and Cp species were found experimentally[28] in the range of 120−180 kcal mol^{-1}. On the other hand, the experimental[29] heterolytic dissociation enthalpies of the neutral Cp_2V, Cp_2-Mn, Cp_2Fe, and Cp_2Ni complexes to M^{2+} and $2Cp^-$ species are 625, 584, 662, and 686 kcal mol^{-1}, respectively. As expected, the heterolytic bond dissociation enthalpies are larger than the corresponding homolytic ones. Moreover, the structural changes on the pentazolato ligand introduced upon coordination strongly suggest significant metal−ligand interactions in the complexes.

The heterolytic dissociation of one of the pentazolato ligands in $M(N_5)_2$ complexes yields the cationic $[MN_5]^+$ species, which prefer to adopt the conformation with the pentazolato ligand in an η^2-bonding mode.

Selected geometric parameters for the cationic $[MN_5]^+$ species computed at the B3LYP/6-31G(d,p) level of theory are shown in Figure 2.

It can be seen that for the $[VN_5]^+$, $[CrN_5]^+$, and $[FeN_5]^+$ species local minima corresponding to the conformation with the pentazolato ligand in an η^5-bonding mode have also been located on the PES at 14.0, 24.0, and 4.8 kcal mol^{-1} higher in energy with respect to the global minima corresponding to the η^2-bonding mode, respectively. The $[MnN_5]^+$ species adopts only the conformation with an η^2-N_5 ligand, while for the $[NiN_5]^+$ species a local minimum corresponding to the conformation involving an η^1-N_5 ligand at 11.7 kcal mol^{-1} higher in energy was located in the PES.

Table 2. Bond Dissociation Enthalpies ΔH_1 and ΔH_2 (in kcal mol^{-1}) of the First Row Transition Metal Monopentazolato Cationic Complexes Computed at the B3LYP/6-31G(d,p) Level

compound	state	ΔH_1	ΔH_2
$[V(\eta^2\text{-}N_5)]^+$, **9**	$^4B_2$	102.3	353.5
$[V(\eta^5\text{-}N_5)]^+$, **10**	$^4E_2$	88.3	339.5
$[Cr(\eta^2\text{-}N_5)]^+$, **11**	$^3B_2$	51.0	353.2
$[Cr(\eta^5\text{-}N_5)]^+$, **12**	$^3E_2$	26.9	329.1
$[Mn(\eta^2\text{-}N_5)]^+$, **13**	$^6A_1$	68.5	326.1
$[Fe(\eta^2\text{-}N_5)]^+$, **14**	$^1A_1$	23.8	278.2
$[Fe(\eta^5\text{-}N_5)]^+$, **15**	$^1A_1$	19.3	273.6
$[Co(\eta^2\text{-}N_5)]^+$, **16**	$^2B_1$	89.1	317.7
$[Ni(\eta^1\text{-}N_5)]^+$, **17**	$^1B_1$	62.2	340.4
$[Ni(\eta^2\text{-}N_5)]^+$, **18**	$^1B_1$	70.2	348.4

Table 3. Valence Shell Electron Configurations for the Bispentazolato, $M(N_5)_2$ Complexes Computed at the B3LYP/6-31G(d,p) Level

$M(N_5)_2$	sym-metry	valence electrons	state	electron configuration
$V(\eta^5\text{-}N_5)_2$	D_{5h}	15	$^4A_1'$	$(a_1')^2(a_2'')^2(e_1'')^4(e_1')^4(a_1)^1(e_2')^2$
$Cr(\eta^5\text{-}N_5)_2$	C_1	16	^3A	$(a)^2(a)^2(a)^2(a)^2(a)^2(a)^2(a)^2(a)^1(a)^1$
$Mn(\eta^2\text{-}N_5)_2$	D_{2d}	17	$^6A_2$	$(b_2)^2(e)^4(e)^4(e)^3(e)^2(a_1)^1(b_2)^1$
$Fe(\eta^5\text{-}N_5)_2$	D_{5d}	18	$^1A_{1g}$	$(a_{1g})^2(a_{2u})^2(e_{1g})^4(e_{1u})^4(a_{1g})^2(e_{2g})^4$
$Co(\eta^5\text{-}N_5)_2$	C_1	19	^2A	$(a)^2(a)^2(a)^2(a)^2(a)^2(a)^2(a)^2(a)^2(a)^2(a)^1$
$Ni(\eta^3\text{-}N_5)_2$	C_{2h}	20	^1A_g	$(b_u)^2(b_u)^2(b_g)^2(a_g)^2(a_u)^2(b_g)^2(a_u)^2$-$(b_g)^2(a_g)^2(a_g)^2$

Interestingly, in all $M(N_5)_2$ complexes (except $Cr(N_5)_2$) the dissociation of the first N_5^- ligand forces the metal center to get closer to the remaining N_5 ligand. Thus, the computed distances between the transition metal center and the centroid of the aromatic pentazolato ring in the $[M(\eta^5\text{-}N_5)]^+$ species were found to be 1.865, 1.846, and 1.501 Å for **10**, **12**, and **15**, respectively. This could be attributed to the increase of the electrostatic interactions between the central metal ion and the negatively charged N_5^- ligand. The same holds also true for the $[M(\eta^2\text{-}N_5)]^+$ species.

The computed bond dissociation enthalpies for both the homolytic (ΔH_1) and heterolytic (ΔH_2) M−(N_5) dissociation processes are summarized in Table 2.

As expected, the heterolytic bond dissociation enthalpies are larger than the corresponding homolytic ones. Similarly, the heterolytic bond dissociation enthalpies of the second pentazolato ligand amounted to 274−354 kcal mol^{-1}, much larger than those of the first one (158−200 kcal mol^{-1}).

Electronic and Bonding Properties of the Bispentazolato Complexes. In general terms, the electronic ground states of azametallocenes closely resemble those of the corresponding metallocenes. The valence shell electron configurations of the azametallocenes are listed in Table 3.

The open shell azavanadocene with 15 valence electrons has a quartet $^4A_1'$ electronic state for the ground D_{5h} structure with the $(a_1')^2(a_2'')^2(e_1'')^4(e_1')^4(a_1)^1(e_2')^2$ valence shell electron configuration. Azachromocene with 16 valence electrons has a triplet ^3A electronic state for the low symmetry ground C_1 structure. Attempts to identify a local minimum on the PES of azachromocene for the higher symmetry D_{5d} structure under symmetry constraints were unsuccessful. Azamanganocene with 17 valence electrons has a high multiplicity (sextet) $^6A_2$ electronic state for the ground D_{2d} structure. The closed shell azaferrocene with 18 valence electrons has a

(28) Cais, M.; Lupin, M. S. *Adv. Organomet. Chem.* **1970**, *8*, 211.
(29) Ryan, M. F.; Eyler, J. R.; Richardson, D. E. *J. Am. Chem. Soc.* **1992**, *114*, 8611−8619.

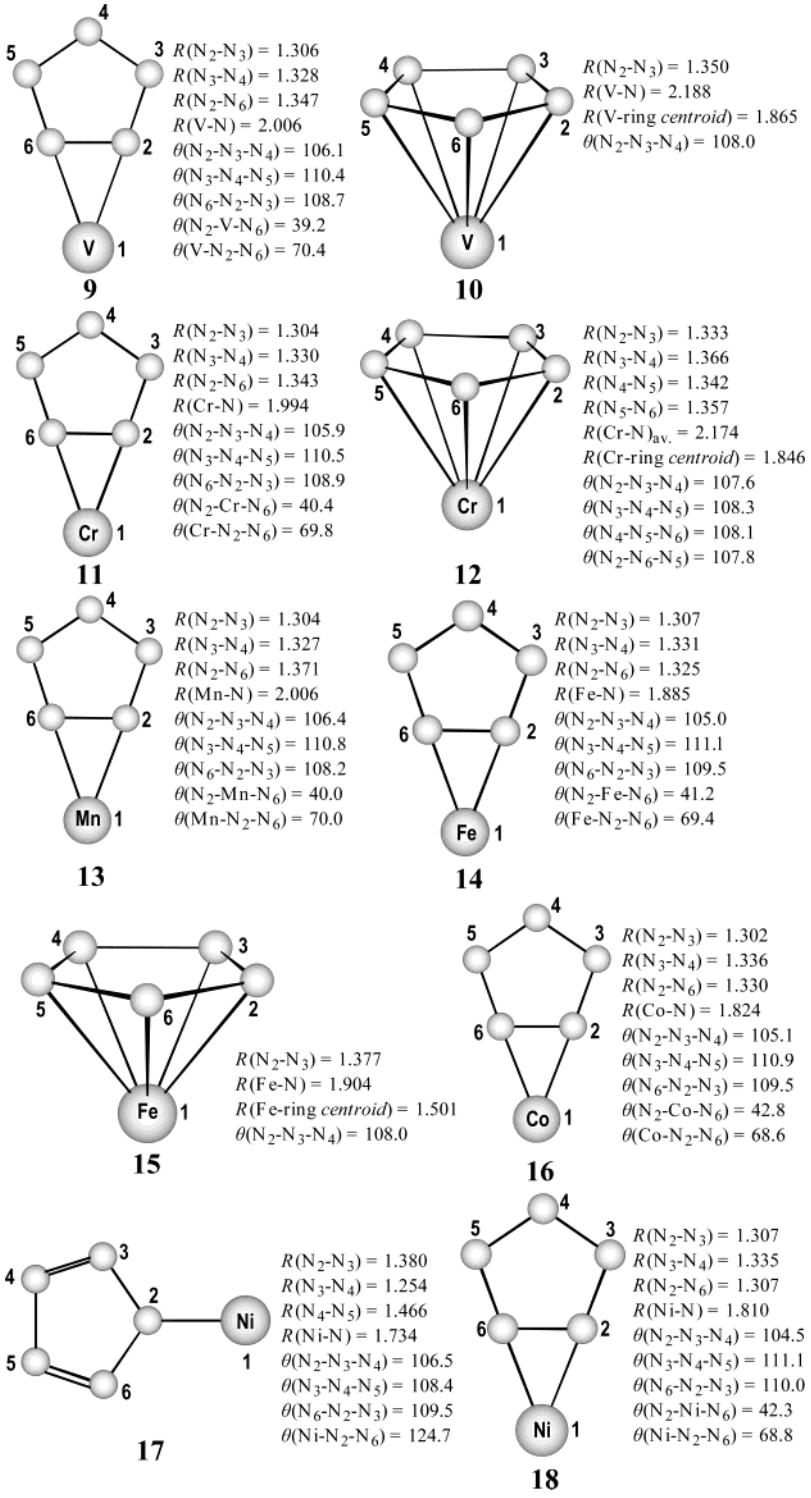

Figure 2. Equilibrium geometries of the first row transition metal monopentazolato cationic complexes computed at the B3LYP/6-31G(d,p) level.

singlet $^1A_{1g}$ electronic state for the ground D_{5d} structure with the $(a_{1g})^2(a_{2u})^2(e_{1g})^4(e_{1u})^4(a_{1g})^2(e_{2g})^4$ valence shell electron configuration resembling that of the ferrocene molecule computed at the B3LYP/DZP level of theory.[14] However, in contrast to ferrocene which adopts the eclipsed D_{5h} ground state in the gas phase,[14] azaferrocene adopts the staggered D_{5d} configuration, while the D_{5h} one corresponds to a transition state, which is only 0.24 kcal/mol higher in energy than the ground D_{5d} configuration. As in the case of azachromocene, azacobaltocene with 19 valence electrons has a doublet ^2A electronic state for the low symmetry ground C_1 structure. Attempts to identify local minima on the PES of azacobaltocene for the higher symmetry D_{5d} and D_{5h} structures under symmetry constraints were unsuccessful. The low symmetry of azacobaltocene is expected on the grounds of the Jahn−Teller effect, because of the singly occupied degenerate e_1'' (for D_{5h}) or e_{1g} (for D_{5d}) molecular orbitals. Finally, azanickelocene with 20 valence electrons has a

Table 4. Mulliken Net Atomic and Natural Charges, Bond Overlap Population (bop), Atomic Spin Density (SD) Distribution, and the Electrophilicity ω (eV) of the Azametallocenes Computed at the B3LYP/6-31G(d,p) Level

$M(N_5)_2$	q(M)	q(N)	bop(M−N)	SD(M)	SD(N)	$\langle S^2 \rangle$	ω[a]
$V(\eta^5\text{-}N_5)_2$	1.46 (0.96)[b]	−0.15 (−0.10)	0.059	2.907	0.009	3.760	3.561
$Cr(\eta^5\text{-}N_5)_2$	1.39 (0.90)	−0.14 (−0.09)	0.071	2.122	0.019	2.035	4.526
$Mn(\eta^2\text{-}N_5)_2$	1.62 (1.25)	−0.31 (−0.20)	0.091	4.876	0.017	8.755	2.035
$Fe(\eta^5\text{-}N_5)_2$	1.20 (0.84)	−0.12 (−0.08)	0.077				4.663
$Co(\eta^5\text{-}N_5)_2$	1.34 (0.77)	−0.13 (−0.08)	0.071	0.955	0.023	0.768	7.374
$Ni(\eta^3\text{-}N_5)_2$	1.26 (0.73)	−0.19 (−0.14)	0.101				9.295
		−0.15 (−0.07)	0.090				
		−0.05 (−0.01)	0.018				
cyclo-N_5^-		−0.20 (−0.20)					0.234

[a] Electrophilicity index $\omega = \mu^2/2\eta$, where μ and η are the chemical potential and hardness, respectively, given approximately by the expressions $\mu = (\epsilon_{LUMO} + \epsilon_{HOMO})/2$ and $\eta = (\epsilon_{LUMO} - \epsilon_{HOMO})$.[30] [b] Figures in parentheses are the Mulliken net atomic charges.

singlet $^1A_{1g}$ electronic state for the ground C_{2h} structure with the $(b_u)^2(b_u)^2(b_g)^2(a_g)^2(a_u)^2(b_g)^2(a_u)^2(b_g)^2(a_g)^2(a_g)^2$ valence shell electron configuration.

Generally, all azametallocenes studied exhibit similar bonding properties. The relevant molecular orbitals (MOs) describing the metal−ligand interactions of representative bispentazolato complexes along with the frontier MOs (FMOs) and the relevant MOs of the free pentazolato ligand are shown in Figure 3.

The metal−ligand orbital interactions for azavanadocene, azachromocene, and azacobaltocene resemble those of the reference azaferrocene complex. Thus, the lowest unoccupied molecular orbitals (LUMOs) of azavanadocene, azachromocene, azaferrocene, and azacobaltocene correspond to antibonding MOs constructed from the out-of phase combination of the π-type LUMO of the pentazolato ligand with the d-type ($3d_{xz}$, $3d_{yz}$) AOs of the central metal atom. The highest occupied molecular orbital (HOMO) of azaferrocene, being a doubly degenerate MO of e_{2g} symmetry, is essentially a nonbonding MO constructed from the $3d_{x^2-y^2}$ and $3d_{xy}$ AOs of Fe with negligible contribution from the π-type orbitals of the pentazolato ligands. These orbitals are singly occupied molecular orbitals (SOMOs) for the open shell azavanadocene, azachromocene, and azacobaltocene complexes. The largest contribution to the bonding metal−ligand interactions comes from the in-phase orbital interaction of the π-type (e_1'') orbitals of the pentazolato ligands with the $3d_{xz}$ and $3d_{yz}$ AOs of the central metal atom. These interactions are described by the HOMO-12,13 for azavanadocene and azachromocene, respectively, the HOMO-13,14 for azaferrocene, and the HOMO-14,15 for azacobaltocene. There are also smaller contributions from the in-phase orbital interactions of the π-type (e_2'') orbitals of the pentazolato ligands with the $3d_{x^2-y^2}$ and $3d_{xy}$ AOs of the central metal atom. These orbital interactions are described by the HOMO-8,9 for azavanadocene, the HOMO-7,9 for azachromocene, the HOMO-9,10 for azaferrocene, and the HOMO-10,11 for azacobaltocene. The bonding metal−ligand orbital interactions of the π-type (a_1' and a_2'') orbitals of the pentazolato ligands with the $3d_{z^2}$ AOs of the central metal atom (HOMO-15, -16, -17, -18 in Figure 2) seem to be negligible.

Let us now go deeper into the electron and spin density distribution of the azametallocenes. The Mulliken and natural bond orbital (NBO) population analysis data along with the atomic spin density distribution and the electrophilicity parameters of the azametallocenes are compiled in Table 4.

It can be seen that there is a significant charge transfer from the pentazolato ligands toward the metal center amounting to 0.54, 0.61, 0.38, 0.80, 0.66, and 0.74 charge unit of natural charge for **3**, **4**, **5**, **6**, **7**, and **8** azametallocenes, respectively. Interestingly, the stronger charge transfer occurs in azaferrocene, while the weaker one occurs in azamanganocene, which involves η^2-bonded pentazolato ligands. According to the bond overlap population (bop) values the metal−ligand bond strength for the η^5-bonded azametallocenes follows the trend Fe−(N_5) > Cr−(N_5) = Co−(N_5) > V−(N_5), which is compatible with the trend followed by the separation distance between the central metal atom and the centroid of the coordinated pentazolato ligand. In the η^2-bonded azamanganocene and the η^3-bonded azanickelocene the metal−ligand interactions are stronger with bop values of 0.091 and 0.101, respectively.

The ligand-to-metal charge transfer (LMCT) renders the aromatic pentazolato ligand more electrophilic; the electrophilicity index ω follows the trend **8** > **7** > **6** > **4** > **3** > **5** ≫ **1**. The ω values for the N_5^- and $N_5^\bullet$ molecules are 0.234 and 2.167 eV, respectively. Moreover, the computed $\langle S^2 \rangle$ values of 3.760, 2.035, 8.755, and 0.768 for **3**, **4**, **5**, and **7**, respectively, indicate (except for **5**) that there is no spin contamination.

Harmonic Vibrational Frequencies of the Bispentazolato Complexes. The most characteristic vibrational modes of the first row transition metal azametallocenes **3**, **4**, **5**, **6**, **7**, and **8**, along with the normal coordinate vectors (arrows), are shown in Schemes 1, 2, 3, 4, 5, and 6, respectively. The harmonic vibrational frequencies and the IR intensities computed at the B3LYP/6-31G(d,p) level of theory are listed in detail in the Supporting Information (Table S1). All these infrared absorption bands could assist in identifying the respective azametallocenes.

For azavanadocene (Scheme 1) the more intense vibrational mode of a_2'' symmetry absorbing at about 358 cm^{-1} is attributed to the N_5-V-N_5 asymmetric stretch. The doubly degenerate vibrational modes of e_1' symmetry at about 99 and 1180 cm^{-1} are assigned to the N_5-V-N_5 bending and *cyclo*-N_5 in-plane stretch modes, respectively.

The symmetric N_5-Cr-N_5 bending mode in azachromocene (Scheme 2) absorbs around 119 cm^{-1}. The more intense vibrational modes in azachromocene absorbing at

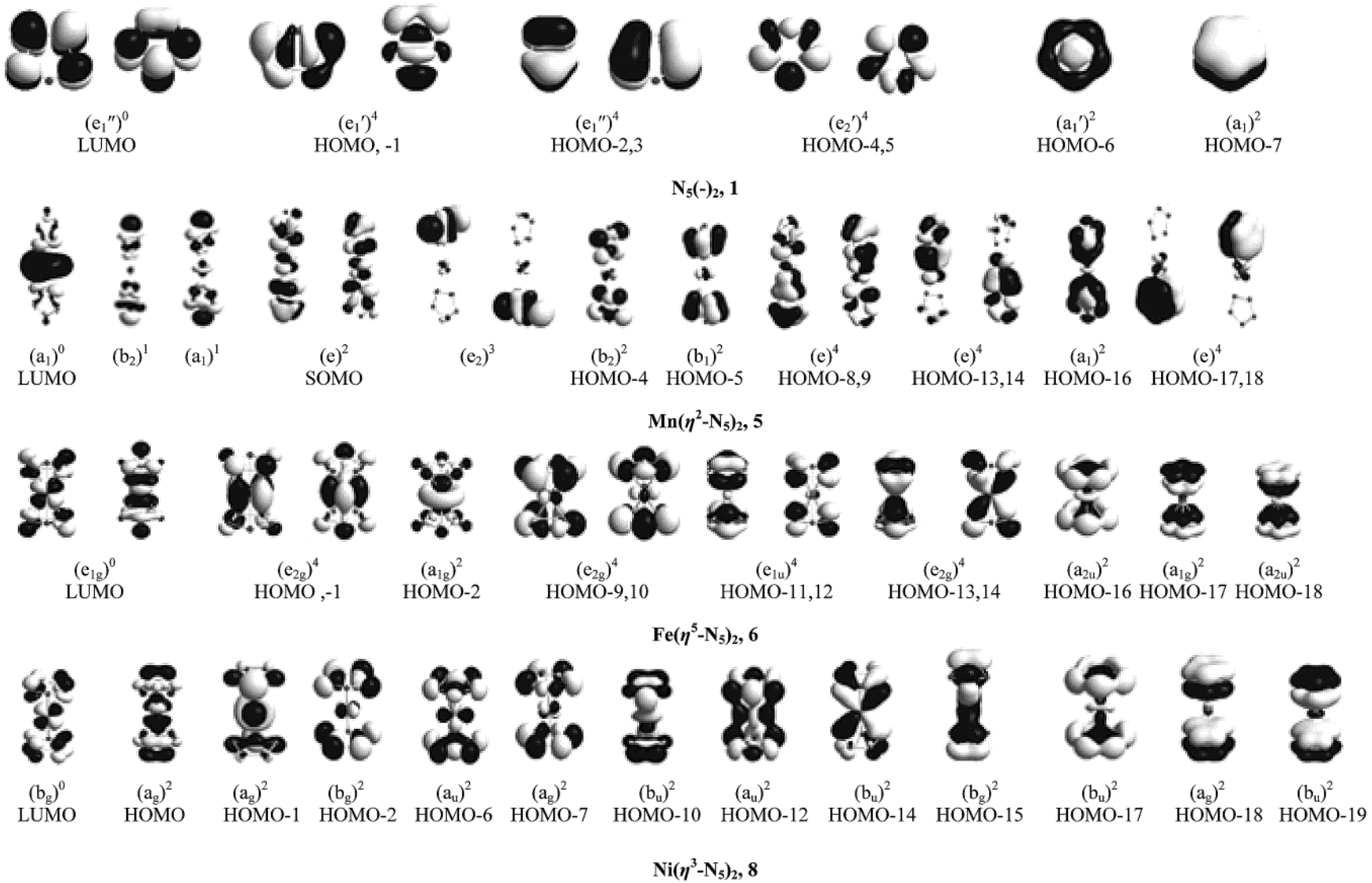

Figure 3. Expanded list of the molecular orbitals of the pentazolato ligand and representative first row transition metal bispentazolato complexes.

Scheme 1

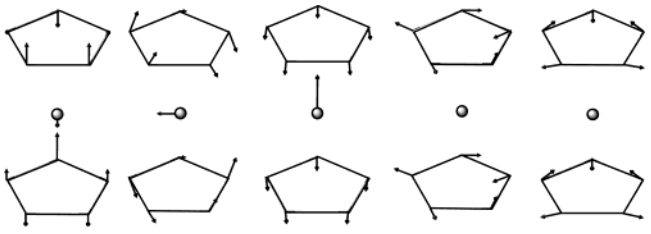

$V(\eta^5\text{-}N_5)_2$, **3**

Scheme 2

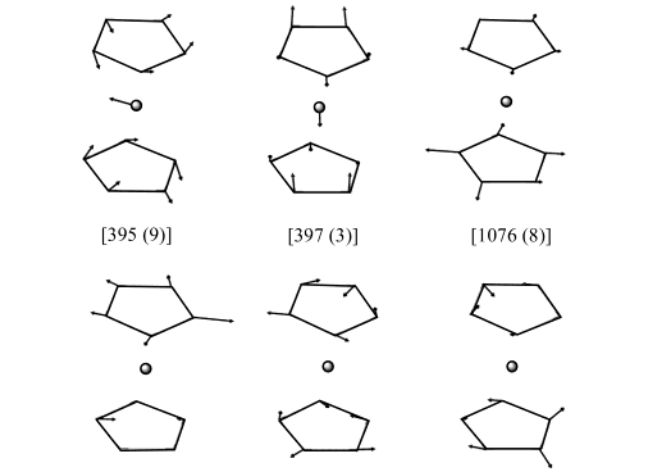

$Cr(\eta^5\text{-}N_5)_2$, **4**

Scheme 3

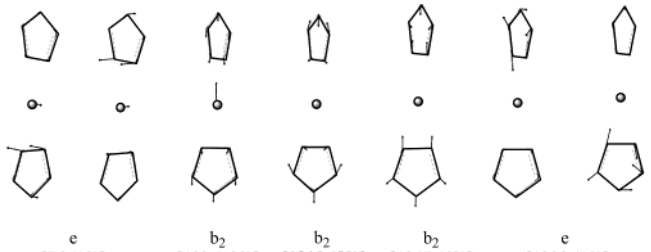

$Mn(\eta^2\text{-}N_5)_2$, **5**

1079, 1131, and 1157 cm^{-1} are attributed to *cyclo*-N_5 in-plane stretching modes of both rings. The vibrational modes at 1076 and 395 cm^{-1} are assigned to the *cyclo*-N_5 breathing and N_5-Cr-N_5 asymmetric bending modes, respectively.

In the azamanganocene (Scheme 3), the more intense vibrational mode of b_2 symmetry absorbing at about 403 cm^{-1} is also attributed to the N_5-Mn-N_5 asymmetric stretch. The next intense vibrational modes in azamanganocene at 1247 and 1218 cm^{-1} are assigned to the *cyclo*-N_5 breathing and in-plane bending modes, respectively. The doubly degenerate vibrational modes at 76 and 1298 cm^{-1} are attributed to $Mn-N_5$ bending and *cyclo*-N_5 in-plane stretching modes, respectively. It is worth noting that both these bands are characteristic of the η^2-bonding mode of the pentazolato ligand, since they are moved toward much lower and much higher frequencies, respectively, with respect to the corresponding bands of the η^5-bonded pentazolato ligand.

Scheme 4

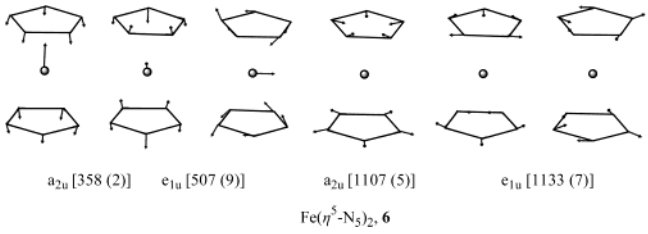

$Fe(\eta^5\text{-}N_5)_2$, **6**

Scheme 5

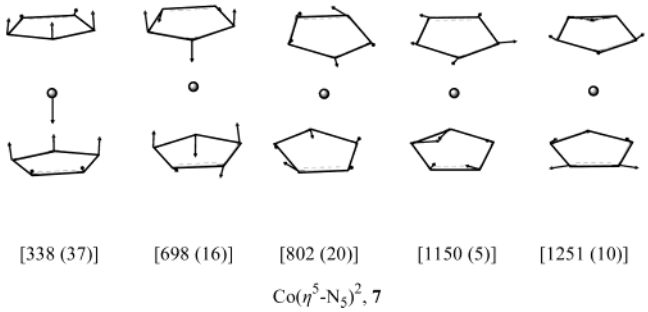

$Co(\eta^5\text{-}N_5)^2$, **7**

It should be noted that the *cyclo*-N_5 in-plane stretching mode of NaN_5, KN_5, MgN_5Cl, and CaN_5Cl complexes involving an η^2-bonded pentazolato ligand were found to absorb at 1289.2, 1281.5, 1305.2, and 1299.6 cm^{-1}, respectively, at the B3LYP/6-311+G(d) level of theory.[12]

For azaferrocene (Scheme 4), the more intense vibrational mode of e_{1u} symmetry due to N_5-Fe-N_5 asymmetric stretching vibration absorbs at about 507 cm^{-1}. The next intense vibrational mode of azaferrocene at 1133 cm^{-1}, exhibiting e_{1u} symmetry, is assigned to the *cyclo*-N_5 in-plane stretching mode of both pentazolato ligands. Moreover, the vibrational modes of a_{2u} symmetry at 1107 and 358 cm^{-1} are attributed to N_5 asymmetric ring breathing and N_5-Fe-N_5 asymmetric stretching modes, respectively. The symmetric *cyclo*-N_5 ring breathing and N_5-Fe-N_5 stretching vibrations absorb at 1099 and 168 cm^{-1}, respectively, while the ring rotation around the main axis absorbs at very low frequency of 168 cm^{-1}.

The asymmetric N_5-Co-N_5 stretching vibration of azacobaltocene (Scheme 5) occurs at 337 cm^{-1}. The vibrational mode at 802 cm^{-1} of azacobaltocene corresponds to a composite vibration involving both *cyclo*-N_5 in-plane and out-of-plane vibrations. The same holds true for the vibrational mode at 1150 cm^{-1}, which involves both *cyclo*-N_5 in-plane and ring breathing vibrations. The high-frequency vibrational mode at 1251 cm^{-1} is attributed to *cyclo*-N_5 in-plane stretching mode of both rings localized on one of the partially double N−N bonds of the pentazolato ligands.

Finally, the more intense b_u vibration mode of azanickelocene (Scheme 6) at 332 cm^{-1} is attributed to the *cyclo*-N_5 out-of-plane topple (N_5 flapping along N_1-N_3). The next intense vibrational mode at 645 cm^{-1} is a composite band involving the asymmetric N_5-Ni-N_5 stretching vibration in conjunction with the asymmetric *cyclo*-N_5 in-plane stretching modes. The vibrational modes at 1045 and 1152 cm^{-1} correspond to the asymmetric and symmetric bending of the η^3-bonded N−N−N moieties, respectively. The

Table 5. The GIAO−B3LYP/6-31G(d,p) ^{14}N NMR Chemical Shifts[a] (δ, ppm) and NICS(0) Values (ppm) of the First Row Transition Metal Bispentazolato Complexes

			^{14}N NMR			
compound	symmetry	state	N1	N2, N5	N3, N4	NICS(0)
cyclo-N_5^-	(D_{5h})	$^1A_1'$	0.6	0.6	0.6	−15.5
cyclo-$N_5^\bullet$	(C_{2v})	$^2A_1$	−37.2	−52.5	−71.2	−19.4
$C_6H_5N_5$	(C_{2v})	$^1A_1$	−76.2	−23.9	16.2	−12.8 (−9.5)[b]
			−80.0[c] (−81.6)[d]	−27.1 (−27.6)	4.9 (4.2)	−37.9
η^5-V(N_5)$_2$	(D_{5h})	$^4A_1'$	2.9	2.9	2.9	35.9
η^5-Cr(N_5)$_2$	(D_{5d})	^3A	12.6	32.5	64.2	
η^2-Mn(N_5)$_2$	(D_{2d})	$^6A_2$	−36.1	11.6, −36.1	27.5, 11.6	−15.8
η^5-Fe(N_5)$_2$	(D_{5d})	$^1A_{1g}$	−69.5	−69.5	−69.5	−69.4
η^5-Co(N_5)$_2$	(D_{5d})	^2A	−65.3	−22.9, −26.3	−23.1, −56.5	−34.9
η^3-Ni(N_5)$_2$	(C_{2h})	^1A_g	143.6	−95.4, 149.3	27.7, −94.8	391.2

[a] The calculated absolute ^{14}N shielding tensor elements σ^{iso} (σ^{aniso}) for the nitromethane, CH_3NO_2, external reference standard at the same level of theory are −117.9 (275.7). [b] NICS(0) value for the benzene ring of phenylpentazole. [c] Experimental chemical shifts for the 4-dimethylaminophenylpentazole taken from ref 31. [d] Experimental chemical shifts for the 4-hydroxyphenylpentazole in parentheses taken from ref 12.

Scheme 6

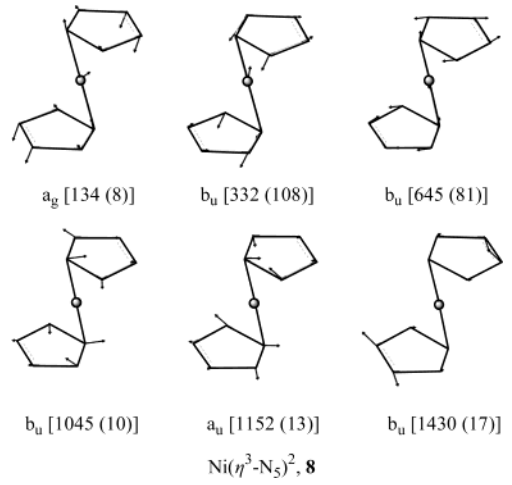

Ni(η^3-N_5)^2, **8**

asymmetric N_5-Ni-N_5 bending vibrational mode absorbs at low frequencies (134 cm^{-1}) while the high-frequency vibrational mode at 1430 cm^{-1} is assigned to the stretching mode of the nonbonded N−N moieties of the pentazolato ligands exhibiting an almost double bond character. The latter band is indicative of the η^3-bonding mode of the pentazolato ligand and therefore could assist in identifying the bonding mode of the pentazolato ligand to a metal atom or ion.

NMR Spectra and Aromaticity of the Bispentazolato Complexes. To assist further the identification of the first row transition metal azametallocenes we present in Table 5 the GIAO-B3LYP/6-31G(d,p)//B3LYP/6-31G(d,p) ^{14}N chemical shifts (δ, ppm), using nitromethane, $MeNO_2$, as an external standard. The reported isotropic chemical shifts were calculated as the difference between the shielding of the reference and the shielding of the molecule of interest, $\delta = \sigma_{ref} - \sigma$. The calculated absolute isotropic shielding tensor elements (σ, ppm) of the azametallocenes are summarized in the Supporting Information (Tables S2). To calibrate the theoretical method the ^{14}N NMR chemical shifts were calculated for the phenylpentazole molecule (C_{2v} point group) and compared to experiment for the 4-hydroxyphenylpentazole[12] and 4-dimethylaminophenylpentazole.[4,31,32] The results are also compiled in Table 4. It can be seen that the computed GIAO-B3LYP/6-31G(d,p)//B3LYP/6-31G(d,p) ^{14}N chemical shifts for N1 and N2,5 of the 4-hydroxy- and 4-dimethylamino-phenylpentazoles are in good agreement with experiment.

For the anionic free pentazolato ligand only one ^{14}N NMR signal is predicted having a chemical shift of $\delta = 0.6$ ppm. However, there are three distinct N atoms in the pentazolate radical, namely, N1, N2,5, and N3,4 having chemical shifts of −37.5, −52.5, and −71.2 ppm, respectively. Obviously, the strong deshielding of the ^{14}N NMR chemical shifts in the radical is due to the decrease of the electron density upon removing one electron from the anionic species. The deshielding effect reflects the decrease of the electron density on the N1, N2,5, and N3,4 atoms which acquire −0.02, −0.001, and 0.02 unit of natural charge. In the phenylpentazole molecule the N1 atom directly bonded to the phenyl group is deshielded, while the N2,5 atoms are shielded with respect to the corresponding atoms in the *cyclo*-N_5 radical, following the electron density distribution of −0.01 and −0.06 charge unit of natural charge on the respective atoms. It should be noted that the strong shielding of the N3,4 atoms in phenylpentazole does not match with the electron density distribution of −0.08 charge unit of natural charge on these atoms. This is also the case for the chemical signals of the respective N atoms in 4-hydroxy- and 4-dimethylamino-phenylpentazoles having experimentally determined[12,31] chemical shifts of 4.2 and 4.9 ppm, respectively. The perfect planarity and the equivalence of the N−N bonds of the anionic pentazolato ligand are indicative of the aromatic character of the ligand. This is further substantiated by the computed nucleus-independent chemical shift (NICS), the magnetic criterion proposed by Schleyer et al.[33] for the aromaticity/antiaromaticity concept. Both *cyclo*-N_5^- and *cyclo*-$N_5^\bullet$ molecules are aromatic with NICS(0) values of −15.5 and −19.4 ppm, thereby exhibiting aromaticity higher than that of benzene (NICS = −7.9 ppm at the same level of theory). Noteworthy is the higher aromaticity of the

(30) Parr, R. G.; v. Szentpály, L.; Liu, S. *J. Am. Chem. Soc.* **1999**, *121*, 1922.
(31) Müller, A.; Wallis, J. D.; Philipsborn, W. v. *Angew. Chem., Int. Ed. Engl.* **1985**, *24*, 513−515.
(32) Butler, R. N.; Fox, A.; Collier, S.; Burke, L. A. *J. Chem. Soc., Perkin Trans. 2* **1998**, 2243.
(33) Schleyer, P. v. R.; Maerker, C.; Dransfeld, A.; Jao, H.; Homes, N. v. E. *J. Am. Chem. Soc.* **1996**, *118*, 6317.

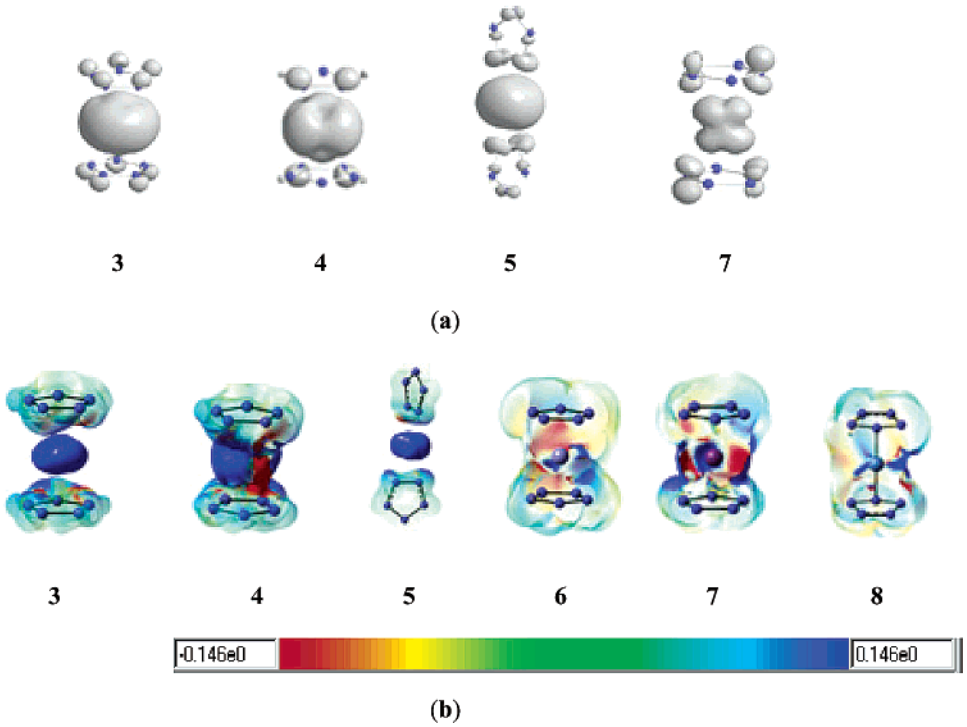

Figure 4. Total atomic spin density surfaces (a) along with the shielding densities on the central metal ion mapped on the current density surfaces (b) for the first row transition metal bispentazolato complexes computed at the B3LYP/6-31G(d,p) level.

pentazolato than the benzene ring in phenylpentazole with NICS(0) values of −12.8 and −9.5 ppm, respectively.

Upon coordination of the pentazolato ligand to the first row transition metal ions there is a significant charge and spin density redistribution on the coordinated ligand, which introduces significant shielding and deshielding effects on the ^{14}N NMR chemical shifts depending on both the nature of the transition metal ion and the coordination bonding mode of the ligand. The total spin density surfaces (SDS) along with the shielding density on the central transition metal ion mapped on the current density of the open shell systems are shown in Figure 4.

Thus, for azavanadocene there is a small shielding effect on all N atoms amounting to 2.3 ppm relative to the free ligand. This shielding effect could not be accounted for by the electron density distribution on the N atoms of the coordinated ligand, which is lower than that in the free ligand. However, there is a small spin density distribution on the coordinated ligand (Table 4), which might be responsible for the introduced shielding effect. The shielding effect is much higher in azachromocene, amounting to 12.0, 31.9, and 63.6 ppm for the N1, N2,5, and N3,4 atoms, respectively, reflecting the spin density distribution on the respective N atoms of the coordinated pentazolato ligand. Noteworthy is the higher shielding of the central metal ion in azachromocene than in azavanadocene.

In the rest of the azametallocenes there is a strong deshielding of the N atoms reflecting the electron and spin density distribution. Interestingly, the aromaticity of the pentazole ring increases significantly upon coordination of the ligand with V^{2+} ion. The same holds true for the pentazole ring in azaferrocene and azacobaltocene; the former exhibits the highest aromaticity, being about twice the aromaticity of the latter. Moreover, the η^2-bonded pentazolato ligand in azamanganocene keeps the aromatic character of the free ligand. However, in azachromocene and azanickelocene the pentazole ring becomes strongly antiaromatic. The strong antiaromaticity of the pentazole ring in azanickelocene being a consequence of the nonplanarity of the ring is indicative of the η^3-bonding mode of the ligand; an η^3-bonded (allyl-type) pentazolato ligand can be viewed as a loose association of an azide ligand with dinitrogen. The azide complexes of Ni^{2+} will be discussed later on.

Electronic Spectra of the Bispentazolato Complexes. The principal singlet−singlet electronic transitions, excitation energies, and oscillator strengths of the first row transition metal azametallocenes calculated with the TD-DFT, B3LYP/6-31G(d,p) method are given in Table 6.

For the free pentazole molecule the first nine computed excited states give rise to the forbidden electronic transitions $e_1' \leftarrow e_2''$ ($n \leftarrow \pi^*$) at 188.0 and 186.5 nm, $e_2' \leftarrow e_2''$ ($\pi \leftarrow \pi^*$) at 165.7, $e_1'' \leftarrow e_2''$ ($\pi \leftarrow \pi^*$) at 165.0, and $a_2'' \leftarrow e_2''$ ($\pi \leftarrow \pi^*$) at 161.5 nm. The electronic transition at 165.0 nm is an allowed transition polarized in the plane of the anion, giving an oscillator strength of 0.0631 au. In this case the direct product $e_1'' \times e_2'' = E_2' + E_1'$, with the E_1' state transforming like (x,y). In the framework of the nine state TD-DFT calculations for the azametallocenes the intraligand ($L \leftarrow L^*$) transitions were not found. In contrast, for all azametallocenes, both charge transfer (CT) either ligand-to-metal (LMCT) or metal-to-ligand (MLCT) and ligand field ($d \leftarrow d$) transitions were able to be identified in the nine excited state TD-DFT calculations.

LMCT transitions for azavanadocene, azamanganocene, azaferrocene and azanickelocene were found at 275−280, 248−277, 259 and 340−350 nm, respectively. Notice that

Table 6. B3LYP/6-31G(d,p) Singlet−Singlet Electronic Transitions, Excitation Energies (eV and nm), and Oscillator Strengths (*f*) of the First Row Transition Metal Bispentazolato Complexes

compound	excited state	transitions	energy (wavelength)	*f*
η^5-V$(N_5)_2$, **3**	1,2	$e_2' \leftarrow e_1''$	1.41 (877)	0.0000
	3,4	$a_1' \leftarrow e_1''$	1.65 (752)	0.0000
	5,6	$a_1' \leftarrow e_1''$	2.34 (530)	0.0000
	7,8	$e_2' \leftarrow e_2''$	4.43 (280)	0.0000
	9	$e_2' \leftarrow e_2''$	4.51 (275)	0.0000
η^5-Cr$(N_5)_2$, **4**	5,6	somo ← lumo	1.68 (739)	0.0000
	7	homo-2 ← lumo	2.05 (605)	0.0000
	8	homo-2 ← lumo + 1	2.06 (601)	0.0000
	9	homo-2 ← lumo	2.70 (460)	0.0000
η^2-Mn$(N_5)_2$, **5**	1	$b_2 \leftarrow a_1$	4.47 (277)	0.0001
	2	$a_1 \leftarrow a_1$	4.64 (267)	0.0000
	3,4	$e \leftarrow a_1$	4.66 (266)	0.0010
	5	$b_2 \leftarrow a_1$	4.96 (250)	0.0001
	6	$a_1 \leftarrow a_1$	4.96 (250)	0.0000
	7,8	$e \leftarrow a_1$	4.97 (250)	0.0003
	9	$b_2 \leftarrow a_1$	5.00 (248)	0.0189
η^5-Fe$(N_5)_2$, **6**	1,2	$e_{2g} \leftarrow e_{1g}$	1.67(743)	0.0000
	3,4	$a_{1g} \leftarrow e_{1g}$	1.97 (624)	0.0000
	5,6	$a_{1g} \leftarrow e_{1g}$	2.92 (425)	0.0000
	7,8,9	$e_{1g} \leftarrow e_{1g}$	4.79 (259)	0.0000
η^5-Co$(N_5)_2$, **7**	7	somo ← lumo + 1	1.50 (827)	0.0000
	8	homo-7 ← lumo	1.68 (738)	0.0000
	9	homo-1 ← lumo + 1	2.16 (575)	0.0000
η^3-Ni$(N_5)_2$, **8**	4	$a_g \leftarrow b_g$	1.55 (802)	0.0000
	5	$b_g \leftarrow b_g$	2.45 (506)	0.0001
	6	$a_u \leftarrow b_g$	2.55 (487)	0.0090
	7	$a_u \leftarrow b_g$	3.54 (350)	0.0414
	8	$b_u \leftarrow b_g$	3.60 (344)	0.0001
	9	$a_g \leftarrow b_g$	3.65 (340)	0.0000

the ligand-to-metal CT transitions in NaN_5, KN_5, and CaN_5-Cl compounds are predicted to absorb in the region of 200−260 nm.[12] On the other hand, the MLCT and d ← d transitions were found in the visible region of the spectra at 530−577, 601−739, 425−743, 575−827, and 487−802 nm for **3**, **4**, **6**, **7**, and **8**, respectively. For azachromocene, azacobaltocene, and azanickelocene complexes electronic transitions absorbing in the near-infrared region of the spectra were also predicted at 1411−2840, 1101−2320, and 1145−1390 nm, respectively. The origin of the low-energy near-IR bands is the electronic transitions from "nonbonding" d orbitals to "antibonding" M−L molecular orbitals and the intervalence ligand-to-ligand charge transfer (LLCT) transitions.

Seeking Synthetic Routes to Azametallocenes. Among the first row transition metal azametallocenes studied we selected azanickelocene to explore possible synthetic routes. Our choice was based on (i) the geometric and electronic structure of azanickelocene involving an η^3-bonded *cyc*-N_5^- ligand, which can be considered to result from the interaction of an η^3-bonded azide ligand with dinitrogen; (ii) the tendency of nickel to form easily complexes with allyl-type ligands; and (iii) the ability of nickel(0) complexes to afford oxidative addition reactions resulting in the rupture of relatively strong bonds, such as H−H, C−C, and C−N bonds. The last point is related with the existence and stability of substituted pentazole ring compounds, such as the Ugi−Huisgen-type arylpentazoles,[34−39] which are easily accessible. Using negative-ion electrospray ionization mass spectrometry (ESI-MS-MS) the substituted arylpentazoles are

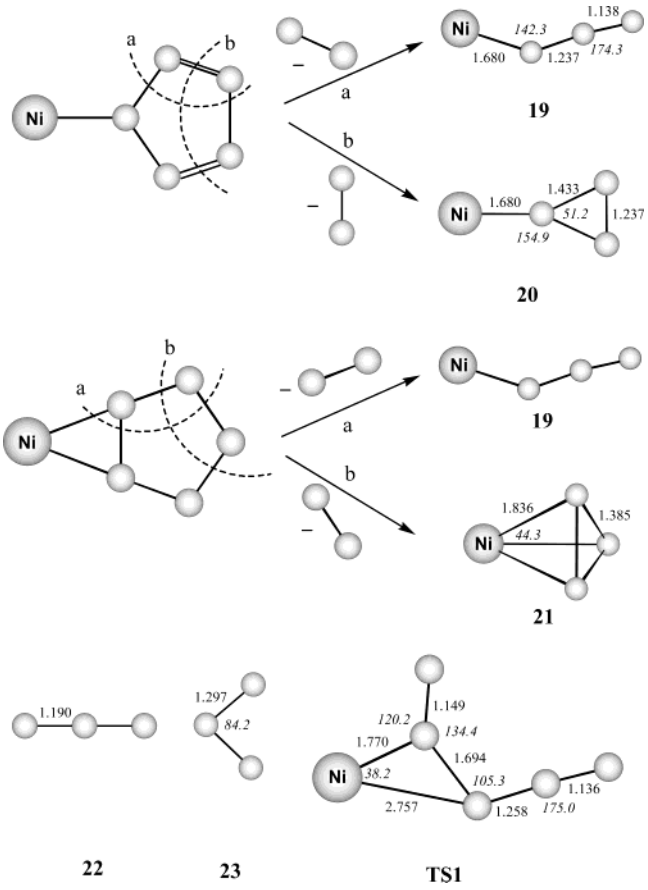

Figure 5. Equilibrium geometries of the stationary points along the reaction pathway of dinitrogen dissociation from the $[Ni(N_5)]^+$ complex computed at the B3LYP/6-31G(d,p) level.

easily fragmented either to arylazides (at low collision voltage) or to the pentazole anion (at high collision voltage).[1]

Cycloaddition of Dinitrogen to a Coordinated Azide Ligand. Let us first examine the reaction of dinitrogen with a nickel(II) azide complex. Searching the PES of the $[Ni,N_3]^+$ system we located the global minimum corresponding to Ni(η^1-N_3)]$^+$ species, **19**, involving an end-on coordinated linear azide ligand, as well as two local minima corresponding to structures involving either an η^1- or an η^3-bonded cyclic azide ligand (Figure 5). The [Ni(η^1-*cyc*-N_3)]$^+$ complex, **20**, resulting upon dinitrogen dissociation from the [Ni(η^1-N_5)]$^+$ complex was found at 34.7 kcal mol^{-1} higher in energy than the ground-state [Ni(η^1-N_3)]$^+$ complex. On the other hand, the [Ni(η^3-*cyc*-N_3)]$^+$ complex, **21**, resulting from the [Ni(η^2-N_5)]$^+$ complex upon detachment of a dinitrogen

(34) (a) Huisgen, R.; Ugi, I. *Angew. Chem.* **1956**, *68*, 705. (b) Huisgen, R.; Ugi, I. *Chem. Ber.* **1957**, *90*, 2914. (c) Ugi, I.; Huisgen, R. *Chem. Ber.* **1958**, *91*, 531. (d) Ugi, I.; Perlinger, H.; Bechringer, L. *Chem. Ber.* **1958**, *91*, 2324. (e) Ugi, I. *Angew. Chem.* **1961**, *73*, 172.
(35) Wallis, J. D.; Dunitz, J. D. *J. Chem. Soc., Chem. Commun.* **1983**, 910.
(36) Witanowski, M.; Stefaniak, L.; Janewszewski, H.; Bahadur, K.; Webb, G. A. *J. Cryst. Mol. Struct.* **1975**, *5*, 137.
(37) Müller, R.; Wallis, J. D.; Philipsborn, W. v. *Angew. Chem., Int. Ed. Engl.* **1985**, *24*, 513.
(38) (a) Butler, R. N.; Collier, S.; Fleming, A. F. M. *J. Chem. Soc., Perkin. Trans. 2* **1996**, 801. (b) Butler, R. N.; Fox, A.; Collier, S.; Burke, L. A. *J. Chem. Soc., Perkin. Trans. 2* **1998**, 2243. (c) Burke, L. A.; Butler, R. N.; Stephens, J. C. *J. Chem. Soc., Perkin. Trans. 2* **2001**, 1679.
(39) Biesemeier, F.; Müller, U.; Masa, W. *Z. Anorg. Allg. Chem.* **2002**, *628*, 1933−1934.

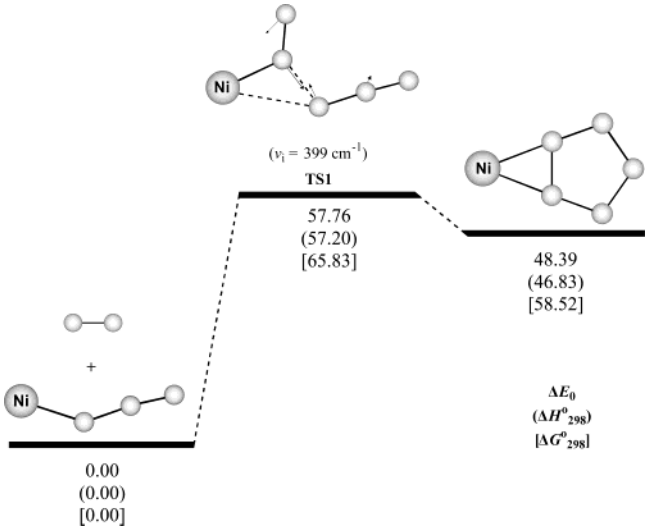

Figure 6. Geometric and energetic reaction profile of cycloaddition of dinitrogen to an azide ligand coordinated to nickel(II), computed at the B3LYP/6-31G(d,p) level.

moiety was found at 15.6 kcal mol^{-1} higher in energy than the ground-state [Ni(η^1-N$_3$)]$^+$. The calculated B3LYP/6-31G(d,p) equilibrium geometry of the free azide ligand is also shown in Figure 5. The global minimum corresponds to the linear geometry of the free azide ligand, **22**, while a bend structure, **23**, was also found as local minimum in the PES at 71.47 kcal mol^{-1} higher in energy. The computed binding energy of the azide ligand with Ni^{2+} dication was found to be 390.35 kcal mol^{-1} at the B3LYP/6-31G(d,p) level of theory.

Dinitrogen dissociation from the [Ni(η^1-N$_5$)]$^+$ complex could afford either **19** or **21**. The first fragmentation pattern corresponds to the detachment of the N$_4$−N$_5$ moiety involving rupture of the N$_3$−N$_4$ and N$_5$−N$_6$ bonds, while the second one corresponds to the detachment of the N$_5$−N$_6$ moiety involving rupture of the N$_2$−N$_6$ and N$_4$−N$_5$ bonds (Figure 2). Both fragmentations are exoergic with exothermicities of 60.10 and 25.35 kcal mol^{-1}, respectively. The higher energy demand of the former process could be accounted for well by the stronger N−N bonds to be ruptured. The relatively low exothermicity of the latter process indicates that the [Ni(η^1-N$_5$)]$^+$ complex should be manageable on a preparative scale. Along this line we investigated the possible catalytic role of Ni^{2+} dication in the addition of dinitrogen to azide to yield the desired pentazolato ligand. The geometric and energetic reaction profile is depicted schematically in Figure 6, while the equilibrium structures of the stationary points along the reaction pathway are shown in Figure 5.

It can be seen that the [2 + 3] cycloaddition reaction is an endothermic process by 48.39 kcal mol^{-1} in terms of ΔE_0, yielding through the transition state **TS1**, the [Ni(η^2-N$_5$)]$^+$ complex **18**, with a relatively high activation barrier of 57.76 kcal mol^{-1}. The imaginary frequency of **TS1** at 399i cm^{-1} corresponds to the bending of the N−N−N moiety being coordinated to nickel(II). The normal coordinate vectors (arrows) of the vibrational mode are shown in Figure 6. The computed barrier height is somewhat larger than that of 42.06 kcal mol^{-1} for the [2 + 3] cycloaddition reaction between dinitrogen and a free azide anion computed at the CCSD(T)/aug-cc-pVTZ level of theory,[2a] indicating a higher lability (lower kinetic stability) of the coordinated than the free pentazolato ligand. This is further supported by the computed barrier heights for the reverse decomposition reactions of the coordinated and free pentazolato ligand being 9.37 and 27.72 kcal mol^{-1}, respectively. It is worth noting that the barrier heights for the decomposition reactions of an η^2-coordinated pentazolato ligand with the alkali metal cations were found to be 19.9, 22.0, 2.5, and 25.8 kcal mol^{-1} for Li, Na, K, and Rb derivatives, respectively, at the QCISD(T)/6-311+G(d) level of theory.[40] Summing up, the predicted high activation barrier for the [2 + 3] cycloaddition between dinitrogen and azide anion in the presence of Ni^{2+} cations illustrates that this reaction does not seem to provide a promising synthetic route for transition metal pentazolato complexes.

Oxidative Addition of Phenylpentazole and Fluoropentazole to Ni(0) Bisphosphane Complexes. We examined next the oxidative addition reactions of phenylpentazole, **24**, and fluoropentazole, **25**, to $(PH_3)_2Ni(CH_2{=}CH_2)$ complex, **26**, aiming to obtain a coordinated pentazolato ligand with nickel(II) metal center. Phenylpentazole and ring substituted arylpentazoles are well-characterized molecules.[34−39] The crystal structure of phenylpentazole has recently been determined by X-ray crystallography.[39] The B3LYP/6-31G(d,p) optimized geometry of phenylpentazole shown in Figure 7 closely resembles that determined experimentally. On the other hand, very recently[41] the possible existence of FN_5 was studied experimentally and by ab initio electronic structure theory. It was found that fluoropentazole has very limited kinetic stability and therefore could not be observed. Along this line we thought it would be advisable to study the possibility for trapping the unstable fluoropentazole species by a Ni(0) complex making use of its ability to afford oxidative addition reactions resulting in the rupture of the N−F bond. The equilibrium geometries of the stationary points along the reaction pathway involved in the oxidative addition reactions of phenyl- and fluoropentazole to $(PH_3)_2Ni(CH_2{=}CH_2)$ complex computed at the B3LYP/6-31G(d,p) level of theory are given in Figure 7. All attempts to locate transition states for both oxidative addition reactions were unsuccessful. Surprisingly, searching for TS along the reaction pathway of the oxidative addition of phenylpentazole to **26** we located structure **27** at 13.47 kcal mol^{-1} higher in energy with respect to reactants. Interestingly, the equilibrium structure of **27** involves an η^2-benzyne type coordination of the phenylpentazolato ligand through one C=C double bond of the phenyl ring adjacent to a C−N bond with the nickel(II) metal center. In this intermediate the C=C bond coordinated to nickel(II) is lengthened by 0.062 Å with respect to the free phenylpentazolato ligand. The separation distance of 1.792 Å between the centroid of the coordinated C=C double bond of the phenylpentazolato ligand and the

(40) Zhao, J. F.; Li, N.; Li, Q. S. *Theor. Chem. Acc.* **2003**, *110*, 10−18.
(41) Netzloff, H. M.; Gordon, M. S.; Christie, K.; Wilson, W. W.; Vij, A.; Vij, V.; Boatz, J. A. *J. Phys. Chem. A* **2003**, *107*, 6638−6647.

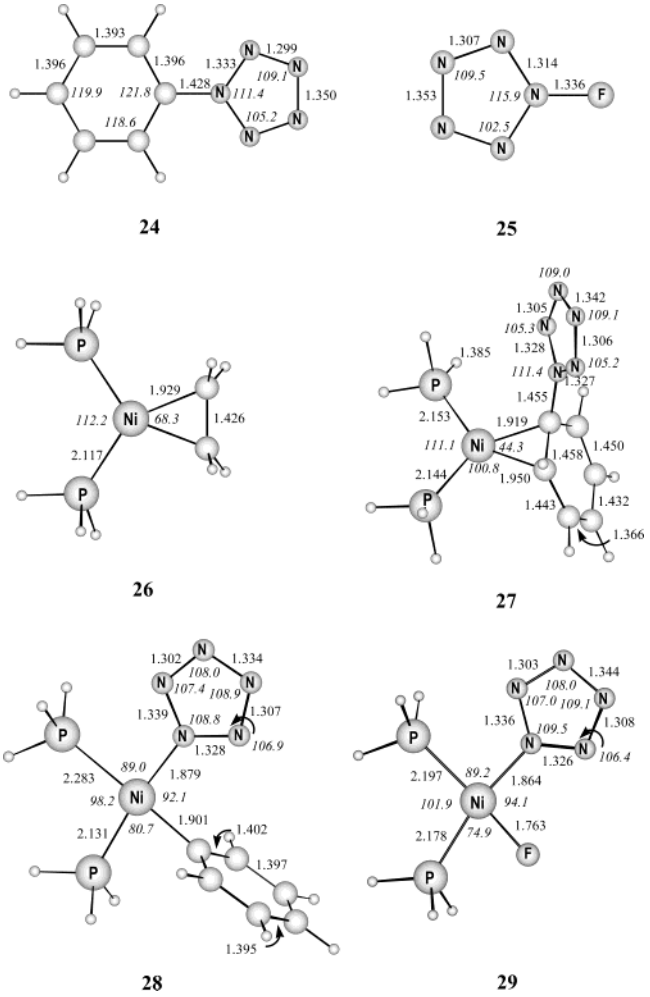

Figure 7. Equilibrium geometries of the stationary points along the reaction pathway of the oxidative addition of phenyl- and fluoropentazole to $(PH_3)_2$-Ni(CH_2═CH_2) complex computed at the B3LYP/6-31G(d,p) level.

nickel(II) central atom is exactly the same as that of the coordinated ethylene ligand in the reactant complex **26**. In the coordinated phenylpentazolato ligand the phenyl ring is not coplanar with the P2NiC2 coordination plane, exhibiting a characteristic folding along the coordinated C═C bond with a flap angle of about 69°. Moreover, the pentazole ring has been tilted along the C_2 axis of the phenyl ring by 21.4° and forms with the C_2 axis an angle of 149.4°. The C−N bond has also been elongated by 0.027 Å, while the nitrogen atom is not coordinated to nickel(II) central atom with the Ni···N separation distance being 2.815 Å.

The formation of the intermediate **27** instead of the expected nonpolar 3-center transition state characterizing the oxidative addition reactions could be explained in terms of the relevant orbital interactions involving the interaction of the HOMO (a nonbonding lone pair 3d orbital) of the $(PH_3)_2$-Ni fragment with the LUMO of the PhN_5 ligand (Scheme 7). The LUMO of PhN_5 ligand corresponds to a π*-type MO which is bonding with respect to the C and N atoms of the C−N bond to be ruptured, but antibonding with respect to the adjacent C−C bonds of the phenyl ring. It can be seen that the favorable HOMO−LUMO orbital interaction is that corresponding to the orientation of the HOMO toward the

Scheme 7

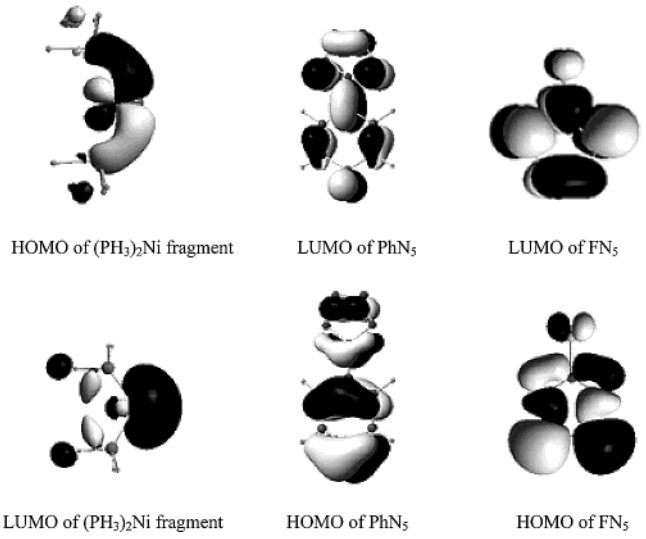

antibonding C−C component of the LUMO resulting in the formation of **27**. This interaction is further enhanced by the concomitant orbital interaction of the LUMO of the metal fragment with the HOMO of the PhN_5 ligand (Scheme 7).

The thermodynamically unstable intermediate **27** can be easily converted to the more stable by 18.15 kcal mol^{-1} final product **28**, with the whole oxidative addition process being slightly exothermic; the exothermicity being 4.69 kcal mol^{-1} in terms of ΔE_0 at the B3LYP/6-31G(d,p) level of theory. In contrast, the oxidative addition of fluoropentazole to **26** yielding **29** is predicted to be strongly exothermic, the exothermicity being 86.23 kcal mol^{-1} in terms of ΔE_0 at the B3LYP/6-31G(d,p) level of theory. This result indicates that the kinetically unstable FN_5 can be trapped by the $(PH_3)_2$-Ni(CH_2═CH_2) complex through the oxidative addition process affording complex **29** involving an η^1-coordinated pentazolato ligand, thus waiting to be made by experimentalists. The higher exothermicity of the oxidative addition reaction of FN_5 with respect to that of PhN_5 could be explained in terms of the strength of the bonds to be ruptured. Thus, the B3LYP/6-31G(d,p) homolytic bond dissociation energy of 71.52 kcal mol^{-1} for the N−F bond in FN_5 is much smaller than the homolytic bond dissociation energy of 114.8 kcal mol^{-1} for the C−N bond in PhN_5. Finally, the nature of the HOMO and LUMO of the FN_5 ligand, both being antibonding with respect to the F−N bond to be ruptured (Scheme 7), accounts well for the direct rupture of the bond without an intervening transition state.

Conclusions

In this paper we have reported a comprehensive DFT study of the structural, energetic, spectroscopic (IR, NMR, UV−vis), electronic and bonding properties of the bispentazolato complexes of the first row transition metals (V, Cr, Mn, Fe, Co, and Ni), the all-nitrogen counterparts of metallocenes. Predictions for possible synthetic routes have also been made.

The results can be summarized as follows:

All first row transition metal pentazolato complexes are predicted to be strongly bound molecules. The computed total

bond dissociation enthalpies that yield free transition metal atoms in their ground states and the free pentazolato ligands were found in the range of 122.0−201.9 (3.7−102.3) kcal mol^{-1} for the bispentazolato (monopentazolato) complexes, while those yielding M^{2+} and anionic pentazolato ligands were found in the range of 473.2−516.7 (273.6−353.5) kcal mol^{-1}.

The calculations predict that the bispentazolato complexes of V^{2+}, Cr^{2+}, Fe^{2+}, and Co^{2+} adopt an equilibrium geometry involving the η^5-bonding mode of the pentazolato ligands with the eclipsed (D_{5h}) conformation for $V(\eta^5\text{-}N_5)_2$ and the staggered (D_{5d}) one for $Cr(\eta^5\text{-}N_5)_2$, $Fe(\eta^5\text{-}N_5)_2$, and $Co(\eta^5\text{-}N_5)_2$. the two pentazolato rings are closer to the Fe^{2+} ion and are perfectly parallel in $V(\eta^5\text{-}N_5)_2$ and $Fe(\eta^5\text{-}N_5)_2$, but slightly tilted in $Cr(\eta^5\text{-}N_5)_2$ and $Co(\eta^5\text{-}N_5)_2$. In contrast to manganocene $MnCp_2$, and nickelocene $MnCp_2$, which have two very low-lying conformations, the eclipsed (D_{5h}) and staggered (D_{5d}) ones, the bispentazolato complex of Mn^{2+} adopts the η^2-bonding mode of the pentazolato ligands with a tetrahedral stereochemistry (D_{2d}), while that of Ni^{2+} adopts an allyl-type η^3-bonding mode with a staggered conformation.

In general terms, the electronic ground states of azametallocenes closely resemble those of the corresponding metallocenes. The valence shell electron configurations and the MO energy levels are important in discussing the bonding characteristics of azametallocenes. The ligand-to-metal charge transfer (LMCT) renders the aromatic pentazolato ligand more electrophilic.

We have also reported the computed spectroscopic properties (IR, NMR, and UV−vis) of azametallocenes in order to assist in identifying the respective azametallocenes and help for future laboratory studies. A complete assignment of the most characteristic infrared absorption bands is given, while the GIAO−B3LYP/6-31G(d,p)//B3LYP/6-31G(d,p) ^{14}N chemical shifts (δ, ppm), using nitromethane, $MeNO_2$, as an external standard, have also been presented, and the aromaticity of the coordinated pentazolato ligand was estimated by making use of the NICS(0) parameter for aromaticity. Moreover, the principal singlet−singlet electronic transitions, excitation energies, and oscillator strengths of the first row transition metal azametallocenes were calculated with the TD-DFT, B3LYP/6-31G(d,p) method.

Finally, seeking synthetic routes to azametallocenes we investigated the geometric and energetic reaction profile of (i) the [2 + 3] cycloaddition of dinitrogen to a coordinated azide ligand with nickel(II) and (ii) the oxidative addition of phenylpentazole and fluoropentazole to Ni(0) bisphosphane complexes. It was found that the first process does not seem to provide a promising synthetic route for transition metal pentazolato complexes, while the second one merits attention for the experimentalists.

Supporting Information Available: The harmonic vibrational frequencies and the IR intensities computed at the B3LYP/6-31G(d,p) level of theory (Table S1). The absolute isotropic shielding tensor elements (σ, ppm) of the azametallocenes computed at the B3LYP/6-31G(d,p) level of theory (Table S2). The Cartesian coordinates and energies of all stationary points (Tables S3−S5). Energetic results (Table S6). This information is available free of charge via the Internet at http://pubs.acs.org.

IC035112G